



HAL
open science

Mechanical noise limit of a strain coupled magneto(elasto)electric sensor operating under a magnetic or an electric field modulation

X. Zhuang, Marc Lam Chok Sing, C. Dolabdjian, Y. Wang, P. Finkel, J. Li,
D. Viehland

► **To cite this version:**

X. Zhuang, Marc Lam Chok Sing, C. Dolabdjian, Y. Wang, P. Finkel, et al.. Mechanical noise limit of a strain coupled magneto(elasto)electric sensor operating under a magnetic or an electric field modulation. *IEEE Sensors Journal*, 2014. hal-01075167

HAL Id: hal-01075167

<https://hal.science/hal-01075167v1>

Submitted on 16 Oct 2014

HAL is a multi-disciplinary open access archive for the deposit and dissemination of scientific research documents, whether they are published or not. The documents may come from teaching and research institutions in France or abroad, or from public or private research centers.

L'archive ouverte pluridisciplinaire **HAL**, est destinée au dépôt et à la diffusion de documents scientifiques de niveau recherche, publiés ou non, émanant des établissements d'enseignement et de recherche français ou étrangers, des laboratoires publics ou privés.

Mechanical noise limit of a strain coupled magneto(elasto)electric sensor operating under a magnetic or an electric field modulation

X. Zhuang, M. Lam Chok Sing, C. Dolabdjian, Y. Wang, P. Finkel, J. Li, and D. Viehland

Abstract—The mechanical noise limit of a strain coupled Magneto(elasto)Electric (ME) composite has been investigated when a magnetic or an electric field modulation is applied to sense a low frequency magnetic field and access DC field measurement capabilities. The sensitivity and noise of such a composite sensor was derived from constitutive equations based on the piezoelectric and ferromagnetic material properties. The analysis was used to evaluate the equivalent noise floor of the composite sensor and to explain the origin of noise by constituting a mechanically coupled electromagnetic model. Experimental measurements revealed a good fit with the proposed model. For example, an equivalent magnetic noise level of ~ 60 pT/Hz @ 1Hz with DC capability was achieved by using an appropriate field modulation.

Index Terms—Magnetolectric effects, Magnetic noise, Signal modulation, Magnetic field sensing

I. INTRODUCTION

MAGNETOELECTRIC (ME) composites have the potential for detecting very small low frequency magnetic fields on the order of a few pT/ $\sqrt{\text{Hz}}$. Passive detection methods are based on the direct strain-coupled ME effect [1], [2]. The detection performance for this passive mode is limited by the dielectric loss contributions to the equivalent noise. In order to avoid this limit, field modulation methods can be applied for magnetic field sensing. The principle of operation is based on the field-dependent couplings between the magnetization, strain and electric polarizations [3], [4], [5].

A ME composite can be driven at a given excitation frequency by using a sine wave magnetic field signal. This field produces both an induced magnetization and an induced strain in the ME composite. This magnetization and strain can be modulated by a low frequency magnetic field via any magnetic, mechanical or electric nonlinearities. First, the induced magnetization is able to produce an electromotive

force in a pick-up coil surrounding the ME composite. Thus, the low frequency magnetic field can be recovered from the pick-up coil by means of a voltage amplifier in association with a synchronous detector. This method is named **M/M**. Secondly, this magnetic field induced strain is transferred to the piezoelectric layers where electric charges are generated. A charge amplifier in conjunction with a synchronous detector serves to recover the low frequency magnetic field from the inter-digital electrodes. This is the **M/E** modulation [6], [7].

Across electrodes deposited on the piezoelectric layer, an electric field can also be applied to drive the ME composite. Serving as an excitation signal, this electric field produces a strain via the piezoelectric effect. This strain can be transferred onto the ferromagnetic layers resulting in a magnetization change (via the 90° domain wall motion). By using a pick-up coil, the induced electromotive-force can be sensed by a voltage amplifier, which is the **E/M** detection mode. This is the converse ME modulation [8], [9]. Finally, the magneto-dielectric (or magneto-capacitance) described as a change in the dielectric constant as a function of an applied magnetic field can also be used for field sensing. In this **E/E** detection mode, low frequency magnetic fields can be measured from the change of the sensor capacitance at a given excitation frequency which is controlled by the low frequency reference magnetic field [10], [11], [12].

II. THEORETICAL ANALYSIS

Illustrated in Fig. 1 is a multi-push-pull structure of a ME composite. The sensing element is made up of two Metglas layers of dimensions $80 \times 10 \times 0.075$ mm³, and a piezoelectric layer of $40 \times 10 \times 0.2$ mm³ with 5 piezoelectric macro-fibers, separated by two Kapton layers. Each Metglas layer is obtained by stacking three foils of $80 \times 10 \times 0.025$ mm³. Inter-digital electrodes are attached on both top and bottom faces of the piezoelectric layer using epoxy resin. The central-to-central space between inter-digital electrodes is 850 μm [13], [14].

Manuscript received Xxxx Xx, 2014.

X. Zhuang, M. Lam Chok Sing and C. Dolabdjian are with the Groupe de Recherche en Informatique, Image, Automatique et Instrumentation de Caen (GREYC), CNRS UMR 6072 – ENSICAEN and the University of Caen, 14050 Caen Cedex, France (e-mail: xzhuang11@yahoo.fr).

P. Finkel is with the Naval Research Laboratory, 4555 Overlook Ave, SW Washington, DC 20375, USA

Y. Wang, J. Li and D. Viehland are with the Materials Science and Engineering Department, Virginia Tech, Virginia 24061, USA.

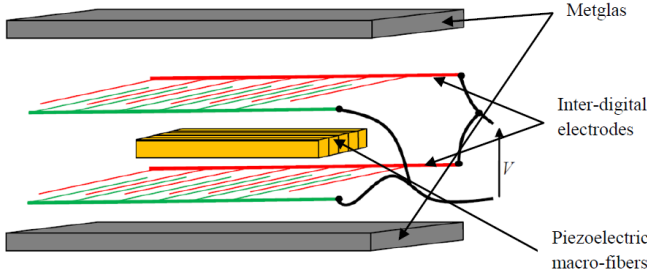


Fig. 1. Sketch view of a multi-push-pull ME composite as a magnetic sensor with inter-digital electrodes

Because the ME composite is fabricated for sensing very low amplitude magnetic signals (\sim pT to nT range), the amplitudes of either the magnetic or the electric excitation field have to be sufficiently strong (\sim μ T magnitude). These implementations result in linear responses for small signals and nonlinear responses for small signal and excitations when used as a mixer. In order to analyze both the linear and nonlinear effects, the constitutive equations for the magnetic, electric and mechanical states are introduced by

$$\begin{cases} D = d_{33,p}T_p + \varepsilon^T E \\ S_p = s_{33}^E T_p + d_{33,p}E \end{cases} \text{ and } \begin{cases} B = d_{33,m}T_m + \mu^T H \\ S_m = s_{33}^H T_m + d_{33,m}H \end{cases}, \quad (1)$$

where E , D , T_p , S_p are the electric field, electric induction, mechanical stress and mechanical strain in the piezoelectric layer; H , B , T_m , S_m are the magnetic field, magnetic induction, mechanical stress and mechanical strain in the ferromagnetic layer; $d_{33,p}$ and s_{33}^E are the piezoelectric and flexibility coefficients in the piezoelectric layer; $d_{33,m}$ and s_{33}^H are the piezomagnetic and flexibility coefficients in the ferromagnetic layer; ε^T and μ^T are the electric permittivity and permeability of the piezoelectric and ferromagnetic layers under a constant stress.

These constitutive equations yield the coupling equations for the magnetic, electric and mechanical parameters in the ME composite [15], [16], [17]

$$\begin{cases} F = \varphi_m H + \varphi_p E \\ j\omega C_{mech}^{EH} \varphi_m F + j\omega (\mu^S H V_m - \Psi l) = 0 \\ j\omega C_{mech}^{EH} \varphi_p F + j\omega (\varepsilon^S E V_p - Q_s l) = 0 \\ j\omega C_{mech}^{EH} F = (v_1 + v_2) \end{cases} \quad (2)$$

The first equation in (2) represents the relation between the mechanical force F , the magnetic field H and the electric field E . Corresponding to a magnetic and an electric field, the force appearing at a given point of the ME composite can be calculated with the magnetoelastic coupling $\varphi_m = \frac{d_{33,m} A_m}{S_{33}^H}$ and

the piezoelectric coupling $\varphi_p = \frac{d_{33,p} A_p}{S_{33}^E}$. A_m and A_p are the

section area of the magnetic and piezoelectric layers, respectively. The second equation binds the mechanical force F , the magnetic field H and the magnetic flux $\Psi (= B \times A_m)$ in the ferromagnetic layers. The coefficient μ^S is the permeability under a constant strain which can be defined by $\mu^S = \mu^T (1 - k_{33,m}^2)$, where $k_{33,m}$ is the elastic coupling

coefficient of the magnetostrictive layer. $C_{mech}^{EH} (= \frac{s_{33}^H l}{A})$ is the mechanical capacity of the ME composite with $s_{33} = \left(\frac{n}{s_{33,m}^H} + \frac{1-n}{s_{33,p}^E} \right)^{-1}$ [18], [19]. n is the ratio between the

ferromagnetic layer thickness and composite layer thickness, defined as $n = t_m / (t_m + t_p)$ where t_m and t_p are the thickness of ferromagnetic and piezoelectric layers; l is the effective length of the ME composite; $A (= A_m + A_p)$ is the section area of the ME composite; and ω is the angular frequency and V_m is the volume of the ferromagnetic layers. Represented in the third equation, is the relation between the mechanical force F , the electric field E and the electric charge Q in the piezoelectric layer. The coefficient ε^S is the permittivity under a constant strain which is defined by $\varepsilon^S = \varepsilon^T (1 - k_{33,p}^2)$ where $k_{33,p}$ is the elastic coupling coefficient of the piezoelectric layer; and V_p is the volume of the piezoelectric layers. The last equation gives the elastic relation between the mechanical force F and the sum of two edge vibration speeds, $(v_1 + v_2)$, along the length direction.

The simplified coupling equations between the magnetic field, the electric field, the electric charge and the magnetic flux can be derived from (2) for investigation of the modulation performances. This yields

$$\begin{cases} \varphi_m \varphi_p C_{mech}^{EH} E + (\varphi_m^2 C_{mech}^{EH} + \mu^S V_m) H - \Psi l = 0 \\ (\varphi_p^2 C_{mech}^{EH} + \varepsilon^S V_p) E + \varphi_m \varphi_p C_{mech}^{EH} H - Q_s l = 0 \end{cases} \quad (3)$$

By applying a magnetic or an electric field wave signal on the composite, the sensitivities (voltage and current detection versus magnetic field excitation, voltage and current detection versus electric field excitation, respectively named **M/M**, **M/E**, **E/M**, **E/E**) can be deduced by the derivative of (3) with respect to the excitation type for a low frequency magnetic field H .

$$\begin{cases} \frac{\partial^2 U}{\partial H_{ex} \partial H} = -\frac{j\omega_{ex}}{l} \left(\frac{\partial \varphi_m^2}{\partial H_{ex}} C_{mech}^{EH} + \varphi_m^2 \frac{\partial C_{mech}^{EH}}{\partial H_{ex}} + \frac{\partial \mu^S}{\partial H_{ex}} V_m \right) \\ \frac{\partial^2 I}{\partial H_{ex} \partial H} = \frac{j\omega_{ex}}{l} \left(\frac{\partial \varphi_m}{\partial H_{ex}} \varphi_p C_{mech}^{EH} + \varphi_m \frac{\partial \varphi_p}{\partial H_{ex}} C_{mech}^{EH} + \varphi_m \varphi_p \frac{\partial C_{mech}^{EH}}{\partial H_{ex}} \right) \\ \frac{\partial^2 U}{\partial E_{ex} \partial H} = -\frac{j\omega_{ex}}{l} \left(\frac{\partial \varphi_m^2}{\partial E_{ex}} C_{mech}^{EH} + \varphi_m^2 \frac{\partial C_{mech}^{EH}}{\partial E_{ex}} + \frac{\partial \mu^S}{\partial E_{ex}} V_m \right) \\ \frac{\partial^2 I}{\partial E_{ex} \partial H} = \frac{j\omega_{ex}}{l} \left(\frac{\partial \varphi_m}{\partial E_{ex}} \varphi_p C_{mech}^{EH} + \varphi_m \frac{\partial \varphi_p}{\partial E_{ex}} C_{mech}^{EH} + \varphi_m \varphi_p \frac{\partial C_{mech}^{EH}}{\partial E_{ex}} \right) \end{cases} \quad (4)$$

The parameters V_m and V_p are the volumes of the ferromagnetic and piezoelectric phase of the ME composite. The first and third equations present the magnetization detected with a coil surrounding the ME composite. The pick-up coil converts the magnetization change into an output voltage following Lenz's law $U(t) = -\frac{\partial \Psi(t)}{\partial t}$, assuming that the output current is null. The second and fourth equations represent the charge detection sensed by the interdigital electrodes of the ME composite. These interdigital electrodes convert the change of electric charges into a current according to the relation $I(t) = \frac{\partial Q(t)}{\partial t}$. In this case, the output voltage is assumed to be null. A charge amplifier is connected to the electrodes to convert the current into an output voltage.

The existence of magnetic domains and their propagation velocity has been predicted in order to explain the magnetization reversal behaviors of ferromagnetic materials [20], [21]. The domain walls can be regarded as magnetic probes for investigating the magnetic behavior of a ferromagnetic material, since they finely change their polarization directions under an external magnetic field. These changes of the magnetic domains can result in net magnetization change in the material. According to Lenz's law, this can give rise to an electromotive force in a pick-up coil wound around the materials. In the conversion process, a magnetic nonlinear response appears between the applied magnetic field and the induced magnetization. This magnetic nonlinearity is defined by the coherence of two magnetic fields or a magnetic field and a stress for a magnetic flux output. A nonlinear factor ν_1 is defined to relate the strength of the coupling between the magnetic field and the magnetic flux density. This magnetic flux density is given as a function of the magnetic excitation. From this curve, the magnetic permeability can be deduced as a function of the low frequency magnetic field.

For a ferromagnetic material, a change in shape can be explained by sample deformation. The latter produces a mechanical strain (and/or stress) in ferromagnetic materials. If we apply a magnetic field on ferromagnetic materials, a deformation appears as a function of this magnetic field, due to 90° domain wall motion. Since the coupling between the applied magnetic field and the induced strain is non-linear, two incoherent magnetic fields can produce a correlated output strain. A nonlinear factor η_1 can be defined to evaluate this coupling strength. This nonlinear factor can be regarded as either the change of the low frequency magnetic transfer function as a function of the applied excitation or the transfer function for the excitation field as a function of the low frequency magnetic field.

The coupling between the magnetic flux and the stress is dominated by the piezomagnetic effect. Unlike magnetostriction, there is a change in sign of the magnetization when an applied external stress changes its direction. The stress induces a magnetization change by producing 90° domain wall motion via the piezomagnetic effect. Another magnetization process occurring by 180° domain wall motion can be given as a function of the amplitude of the magnetic

excitation. These two types of magnetization processes correlate to each other by inducing a coherent output magnetic flux. This coupling can be characterized by a magnetic nonlinear factor η_1^* . The relation between the applied stress and the output magnetic flux density can be influenced by a second stress. Thus, a factor τ_1 is defined to describe the piezomagnetic nonlinearity.

Mechanical nonlinearity is based on a change of the flexibility under a stress oscillation. This effect can be characterized by the measurement of the output coupling strength when applying two incoherent stresses on a sample. A nonlinear factor κ_1 is defined to describe this effect.

The piezoelectric coefficient can change in response to an applied external electric field. This effect is known as the piezoelectric nonlinearity. Therefore, the piezoelectric coefficient, $d_{33,p}$, is a stress dependent parameter. A piezoelectric coefficient, ψ_1 , is introduced to investigate the correlated charge output under two incoherent stresses. An electric polarization change can result in response to either an electric field or an external stress. These two polarizations correlate to each other before converting to an output electric induction. The nonlinear factor, γ_1 , is defined as the nonlinear relationships between the electric excitation and the low frequency stress.

We notice that all these nonlinear relations can be described by a polynomial equation of the form $y = ax \left(1 + \frac{b}{2}x \right)$ where y

can be the strain S , the magnetic flux or the electric charge as a function of either the magnetic field H or stress T represented by x . a and b are the linear coefficient and relative nonlinear factor, respectively. x can be constituted of a low frequency component x_{lf} and an excitation signal x_{ex} . In Table I, we have gathered the nonlinear factors and associated relationships for the different types of operation. A general form of these relations is represented in Fig. 2,

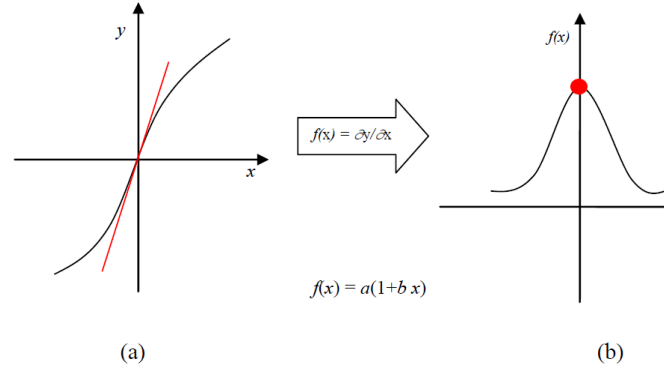


Fig. 2: Nonlinear relation description rule use.

defining a polynomial function with a linear coefficient and nonlinear terms. The red dot in Fig. 2 (b) corresponds to the highest nonlinear coefficient.

Compared to the piezoelectric coupling ϕ_p and the mechanical capacity C_{mech}^{EH} , the magnetoelastic coupling ϕ_m is much more sensitive to an external magnetic field or stress [22], [26]. Therefore, without loss of generality, (4) can be simplified by considering only the dominant terms,

TABLE I
OVERVIEW OF THE NONLINEAR FACTORS AND ASSOCIATED RELATIONS

Type	Function at the working bias point, x_0	Argument	Type of the driving source	Value	Linear coefficient [#]	Non-linear relative factor [#] (first order)	Impacted parameter
Synthesized expression	$f(x) = \frac{\partial y}{\partial x} = a(1 + bx)$	$x = x_f + x_{ex}$	x_{ex}	y	a	$b = \frac{1}{a} \frac{\partial^2 y}{\partial x^2}$	
Magnetic	$\mu^S(H)$	H	H_{ex}	$B \rightarrow \Psi$	μ^S	ν_1	$\frac{\partial \mu^S}{\partial H_{ex}}$
Magnetic	$\mu^S(T)$	T	H_{ex}	$B \rightarrow \Psi$	μ^S	η^*_1	$\frac{\partial \mu^S}{\partial H_{ex}}$
Magnetostrictive	$d_{33,m}(H)$	H	H_{ex}	S	$d_{33,m}$	η_l	$\frac{\partial \varphi_m}{\partial H_{ex}}$
Piezomagnetic	$d^*_{33,m}(T)$	T	$T_{ex} = f(H_{ex})$	$B \rightarrow \Psi$	$d^*_{33,m}$	τ_1	$\frac{\partial \varphi_m}{\partial T_{ex}}$
Mechanical	$s_{33}(T)$	T	$T_{ex} = f(H_{ex}, E_{ex})$	S	s_{33}	κ_1	$\frac{\partial C_{mech}^{EH}}{\partial T_{ex}}$
Piezoelectric	$d_{33,p}(T)$	T	$T_{ex} = f(H_{ex})$	$D \rightarrow Q$	$d_{33,p}$	ψ_1	$\frac{\partial \varphi_p}{\partial T_{ex}}$
Electric	$\varepsilon^S(T)$	T	E_{ex}	$D \rightarrow Q$	ε^S	γ_1	$\frac{\partial \varepsilon^S}{\partial E_{ex}}$

$d^*_{33,m}(T)$ is the piezomagnetic coefficient as a function of the applied stress.

leading to

$$\left\{ \begin{array}{l} \frac{\partial^2 U}{\partial H_{ex} \partial H} = \frac{\omega_{ex}}{l} \frac{\partial \mu^S}{\partial H_{ex}} V_m \\ \frac{\partial^2 I}{\partial H_{ex} \partial H} = \frac{\omega_{ex}}{l} \frac{\partial \varphi_m}{\partial H_{ex}} \varphi_p C_{mech}^{EH} \\ \frac{\partial^2 U}{\partial E_{ex} \partial H} = \frac{\omega_{ex}}{l} \frac{\partial \varphi_m^2}{\partial E_{ex}} C_{mech}^{EH} \\ \frac{\partial^2 I}{\partial E_{ex} \partial H} = \frac{\omega_{ex}}{l} \frac{\partial \varphi_p}{\partial E_{ex}} \varphi_m C_{mech}^{EH} \end{array} \right. \quad (5)$$

By hypothesis, the nonlinearity terms are given by $\frac{\partial \mu^S}{\partial H_{ex}} = \nu_1 \mu^S$, $\frac{\partial \varphi_m}{\partial H_{ex}} = \eta_l \varphi_m$, $\frac{\partial \varphi_m^2}{\partial E_{ex}} = 2\tau_1 \varphi_m \varphi_p$ and $\frac{\partial \varphi_p}{\partial E_{ex}} = \gamma_1 \varphi_p$. Thus, the ME voltage or current coefficients for the modulation methods are

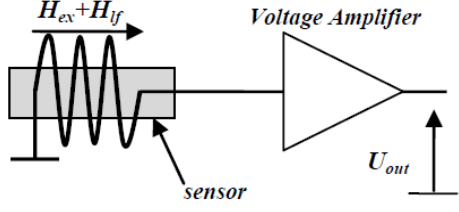
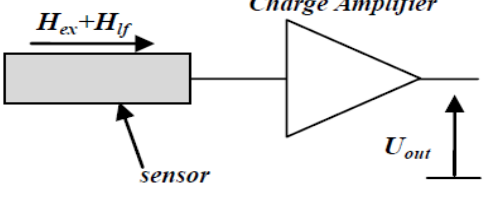
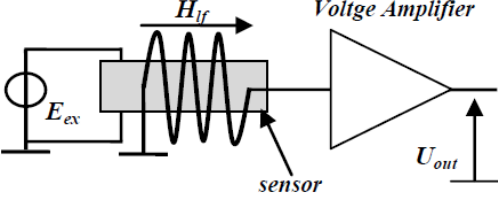
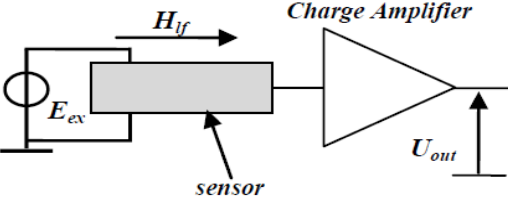
$$\left\{ \begin{array}{l} \alpha_{ME_M/M}^{NL} = \frac{\omega_{ex}}{\mu_0 l} \nu_1 \mu^S V_m \quad \left[\frac{(V/T)}{(A/m)} \right] \\ \alpha_{ME_M/E}^{NL} = \frac{\omega_{ex}}{\mu_0 l} \eta_l \varphi_m \varphi_p C_{mech}^{EH} \quad \left[\frac{(A/T)}{(A/m)} \right] \\ \alpha_{ME_E/M}^{NL} = \frac{\omega_{ex}}{\mu_0 l} (2\varphi_m \tau_1) \varphi_m \varphi_p C_{mech}^{EH} \quad \left[\frac{(V/T)}{(V/m)} \right] \\ \alpha_{ME_E/E}^{NL} = \frac{\omega_{ex}}{\mu_0 l} \gamma_1 \varphi_m \varphi_p C_{mech}^{EH} \quad \left[\frac{(A/T)}{(V/m)} \right] \end{array} \right. \quad (6)$$

Based on our previous work [6], [23], [24], we assume that the thermal induced internal fluctuations in the ferromagnetic and piezoelectric layers can be considered as the main noise sources. The mechanical loss noise limit is the main noise source for a strain coupled ME composite. An application of Nyquist theorem gives the mechanical noise contribution to the output voltage noise spectral density as:

$f_{n_C_{mech}}(f) = \sqrt{4k_B T \tan(\delta_{mech}) / 2\pi f C_{mech}^{EH}}$ where the mechanical loss factor is defined by $\tan(\delta_{mech}) = \frac{s_{33}''}{s_{33}'}$. The noise

transmission can be investigated by supposing that a small low-frequency force is applied on the composite.

TABLE II
POSSIBLE COMBINATIONS OF MAGNETIC OR ELECTRIC FIELD EXCITATIONS WITH MAGNETIZATION OR ELECTRIC CHARGE DETECTIONS

Detection Excitation	Pick-up coil	Trans-impedance amplifier
Magnetic field	 <p>(a)</p>	 <p>(b)</p>
Electric field	 <p>(c)</p>	 <p>(d)</p>

By deriving (2) for an excitation field and a small low frequency force, we obtain the transfer functions for the force noise contribution to the sensed current and voltage output as

$$\begin{cases}
 \left| \frac{\partial^2 U}{\partial H_{ex} \partial F} \right| = \frac{\omega_{ex}}{l} (\varphi_m \kappa_1 + \eta_1^*) \varphi_m C_{mech}^{EH} \\
 \left| \frac{\partial^2 I}{\partial H_{ex} \partial F} \right| = \frac{\omega_{ex}}{l} (\kappa_1 + \psi_1) \varphi_m \varphi_p C_{mech}^{EH} \\
 \left| \frac{\partial^2 U}{\partial E_{ex} \partial F} \right| = \frac{\omega_{ex}}{l} (\kappa_1 + \tau_1) \varphi_m \varphi_p C_{mech}^{EH} \\
 \left| \frac{\partial^2 I}{\partial E_{ex} \partial F} \right| = \frac{\omega_{ex}}{l} (\kappa_1 \varphi_p + \gamma_1) \varphi_p C_{mech}^{EH}
 \end{cases} \quad (7)$$

Therefore, the output voltage and current noise spectral densities are given by

$$\begin{cases}
 e_{n_f_M/M} = \frac{\omega_{ex}}{l} (\varphi_m \kappa_1 + \eta_1^*) \varphi_m C_{mech}^{EH} H_{ex} f_{n_C_{mech}} \\
 i_{n_f_M/E} = \frac{\omega_{ex}}{l} (\kappa_1 + \psi_1) \varphi_m \varphi_p C_{mech}^{EH} H_{ex} f_{n_C_{mech}} \\
 e_{n_f_E/M} = \frac{\omega_{ex}}{l} (\kappa_1 + \tau_1) \varphi_m \varphi_p C_{mech}^{EH} E_{ex} f_{n_C_{mech}} \\
 i_{n_f_E/E} = \frac{\omega_{ex}}{l} (\kappa_1 \varphi_p + \gamma_1) \varphi_p C_{mech}^{EH} E_{ex} f_{n_C_{mech}}
 \end{cases} \quad (8)$$

The equivalent magnetic noise spectral density expressions for the different modulation schemes can be deduced from (6) and (8) in order to evaluate the magnetic detection limits. Taking into account the physical and geometrical parameters of the ME composite, this yields ultimately

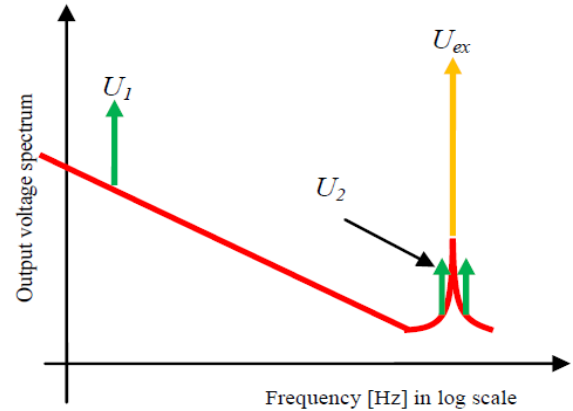


Figure 3: Output spectrum density as a function of frequency and observe classically in the different mode of excitation (M/M, M/E, E/M and E/E). Green, yellow and red lines present respectively the low frequency signal, the carrier and the output voltage noise floor.

$$\left. \begin{aligned}
b_{n_f_M/M}^2 &= \left(\frac{\mu_0 \eta_1 d_{33,m} s_{33}}{\mu^S \nu_1 s_{33,m} A} \right)^2 \left(\frac{4k_B T \tan(\delta_{mech})}{2\pi f \frac{s_{33} l_m}{A}} \right) \\
&= \frac{s_{33}}{A l_m} \left(\frac{\mu_0 \eta_1 d_{33,m}}{\mu^S \nu_1 s_{33,m}} \right)^2 \frac{[4k_B T \tan(\delta_{mech})]}{2\pi f} \\
b_{n_f_M/E}^2 &= \left(\mu_0 \frac{(\kappa_1 + \psi_1)}{\eta_1} \right)^2 \left(\frac{4k_B T \tan(\delta_{mech})}{2\pi f \frac{s_{33} l_p}{A}} \right) \\
&= \frac{A}{s_{33} l_p} \left(\mu_0 \frac{(\kappa_1 + \psi_1)}{\eta_1} \right)^2 \frac{[4k_B T \tan(\delta_{mech})]}{2\pi f} \\
b_{n_f_E/M}^2 &= \left(\mu_0 \frac{(\kappa_1 + \tau_1)}{2\tau_1} \frac{1}{\frac{w l_m d_{33,m}}{s_{33,m}}} \right)^2 \left(\frac{4k_B T \tan(\delta_{mech})}{2\pi f \frac{s_{33} l_m}{A}} \right) \\
&= \frac{1}{s_{33} V_m n} \left(\mu_0 \frac{s_{33,m} (\kappa_1 + \tau_1)}{d_{33,m} 2\tau_1} \right)^2 \frac{[4k_B T \tan(\delta_{mech})]}{2\pi f} \\
b_{n_f_E/E}^2 &= \left(\mu_0 \frac{1}{\frac{w l_m d_{33,m}}{s_{33,m}}} \right)^2 \left(\frac{4k_B T \tan(\delta_{mech})}{2\pi f \frac{s_{33} l_p}{A}} \right) \\
&= \frac{1-n}{s_{33} V_p n^2} \left(\mu_0 \frac{s_{33,m}}{d_{33,m}} \right)^2 \frac{[4k_B T \tan(\delta_{mech})]}{2\pi f}
\end{aligned} \right\} \cdot (9)$$

We notice that all equivalent magnetic noise power spectral densities have a $1/f$ noise behavior and depend on the low frequency loss factors.

III. EXPERIMENTAL RESULTS AND DISCUSSIONS

In order to evaluate the different excitation and detection methods, four experimental setups have been consequently designed for measurements. Table II presents the experimental setup schemes for (a) the magnetization modulation (**M/M**), (b) the direct ME modulation (**M/E**), (c) the converse ME modulation (**E/M**) and (d) the magneto-capacitance modulation (**E/E**). Either a pick-up coil with an associated voltage amplifier or a charge amplifier has been used to measure the electromotive force and generated charge respectively from the magnetic and piezoelectric layers. For all the modulation methods, a low frequency reference magnetic field (2 Hz), produced by a pair of Helmholtz coils, has been applied in the length direction of the ME composite. Thus, the magnetic sensitivity of the sample can be calculated from the ratio of the output signal after the demodulation process to the applied reference magnetic field. The spectrum measurements were made with a HP3562A spectrum analyzer. We notice that for some equivalent magnetic field sensor noise measurements, a reduction of the carrier level is required in order to fit the dynamic range of the spectrum analyzer (~ 90 dB, max value without taking account of a dynamic range reserve).

The attenuation and nonlinearity factors, defined in the theoretical part of this paper, can be measured via the amplitude of the modulation signal appearing around the excitation carrier frequency. A general trend of the observed spectrum near the carrier frequency is given in Fig. 3. We noticed that there exists several attenuations in the measurement system as well as in the ME composite itself. These attenuations may result from the demagnetization, the inter-layer mechanical couplings, the electrode contacts, the detection circuit and the excitation (or pick-up) coil loss. The attenuation and nonlinearity factors can be estimated from the spectrum, by measuring the amplitude of the signals located around the excitation carrier frequency and computing with the relevant parameters of the reference and excitation signals (amplitude, frequency, etc...). First, the attenuation factor can

be deduced from the ratio $\frac{U_{ex}}{U_{ex}^{cal}}$ where U_{ex}^{cal} is the calculated

output voltage amplitude we are expecting for the excitation signal. The second nonlinearity factor is defined as the amplitude ratio of the modulation output signal to the low frequency reference input signal H , per excitation output amplitude, written as $\frac{2U_2}{U_{ex}H}$. In this ratio, we have multiplied

by two in order to standardize the calculations. Thus, the sensitivity model can be constructed by using the coupling parameters, the attenuation factor and the nonlinear factors. The correlation between different detection modes has also been investigated [25]. In these experiments, a strong coherence has been observed between the direct and converse ME modulation modes. However, we did not observe any coherence between the passive and modulation detection methods when they were operated simultaneously. This result confirms that the observed dominant noise source is not due to the passive dielectric loss noise of the sensor.

Table III summarizes the relative nonlinear and attenuation factors for the four modulation modes. The attenuation factors of the magnetic signals for **M/M**, **M/E**, **E/M** and **E/E** modulations are defined as Att_{MM} , Att_{ME} , Att_{EM} and Att_{EE} , respectively. These factors define the energy losses in the magnetoelectric conversion process as well as the difference between the theoretical and practical environment. Similarly, the corresponding attenuation factors for a mechanical force are given by Att_{MFM} , Att_{MFE} , Att_{EFM} and Att_{EFE} . By assuming that the attenuation depends on the excitation method only, we can show that these relations can be simplified as $Att_{MFM} \approx Att_{ME}$, $Att_{MFE} \approx Att_{ME}$, $Att_{EFM} \approx Att_{EM}$ and $Att_{EFE} \approx Att_{EM}$.

By using the **M/M** modulation, only the magnetic layers are used for sensing the low frequency magnetic field. The resulting magnetization is sensed along the longitudinal direction. In this excitation method, there are two parameters responding to the applied magnetic field: the magnetic permeability and the magneto-elastic coefficients because the low frequency magnetic field can influence the strain of the sensor. The first effect is due to the 90° domain wall motion and the other results from the 180° domain wall motion in the ferromagnetic layer along the longitudinal direction [26]. For

TABLE III
COEFFICIENT SYNTHESIS OF THE FOUR MODULATION CONFIGURATIONS

Modulation type		M/M	M/E	E/M	E/E
Nonlinear factor for a magnetic field	$\frac{2U_2}{U_{ex}^{mes} H}$	ν_1	η_1	$2\phi_m\tau_1$	γ_1
Attenuation factor	$\frac{U_{ex}^{mes}}{U_{ex}^{cal}}$	Att_{MM}	Att_{ME}	Att_{EM}	Att_{EE}
Noise transmission mode		M/F/M	M/F/E	E/F/M	E/F/E
Nonlinear factor for a mechanical force	<i>Estimated and calculated</i>	$\phi_m \kappa_1 + \eta_1^*$	$\kappa_1 + \psi_1$	$\kappa_1 + \tau_1$	$\phi_p \kappa_1 + \gamma_1$
Attenuation factor		$Att_{MFM} \approx Att_{ME}$	$Att_{MFE} \approx Att_{ME}$	$Att_{EFM} \approx Att_{EM}$	$Att_{EFE} \approx Att_{EM}$

the magnetization modulation case (**M/M**), the 180° reversible domain wall motion is the dominant effect for the modulation mechanism. This type of magnetic domain motion does not change the sensor geometry when its magnetic property is induced by an external magnetic field.

The relevant coefficients of the **M/M** modulation process are illustrated in Table III. An excitation coil (not represented) is connected to a voltage generator to produce a magnetic excitation field corresponding to the applied voltage $U(H_{ex})$ and a pick-up coil recovering the low frequency signals from the magnetization. As detailed in Fig. 3, the output voltage amplitudes U_{ex} , U_2 and U_1 are the responses corresponding to the excitation oscillation, the modulation and the reference signals, respectively. The transfer function and output voltage noise spectral density can be deduced from

$$Tr_{M/M} = Gv \times N_m \frac{2\pi f_{ex}}{\mu_0 l_m} \nu_1 \mu^S V_m H_{ex} Att_{MM} \quad (10)$$

and

$$u_{n-f-MM} = Gv \times N_m \frac{2\pi f_{ex}}{l_m} (\phi_m \kappa_1 + \eta_1^*) \phi_m C_{mech}^{EH} H_{ex} f_{n-C_{mech}} Att_{MFM} \quad (11)$$

By taking account of the attenuation factor Att_{MM} for the magnetic field transfer function and an attenuation factor Att_{MFM} for the mechanical force.

The equivalent magnetic noise spectral density corresponding to the mechanical noise limit can be expressed by the ratio between the output voltage noise and the transfer function $b_{n-MM} = \frac{u_{n-f-MM}}{Tr_{MM}}$. The nonlinear term ν_1 can be

calculated by $\nu_1 = \frac{H_2}{H_{ex}} / H = \frac{2U_2 / G}{U_{ex} H}$ with the measured

parameters ($Gv = 1$). A low frequency magnetic field was then applied to investigate such a magnetization modulation for several injection amplitudes. From the measurements, there was a gap of several orders of magnitude between the

measurement and the theoretical calculations. We believe that the noise produced by the measurement system is the dominant noise source, exceeding the intrinsic mechanical sensor noise contribution. Thus, the performance of the magnetization modulation can be improved by optimizing the excitation and detection system.

Because of the symmetrical behavior of the magnetic and electric layers in strain-coupled ME composites, the direct and converse ME modulations are theoretically equivalent in sensitivities for low frequency magnetic fields according to previous calculations. The magnetoelastic coupling factor is influenced by the external low frequency magnetic field, via the magnetostrictive coefficient $d_{33,m}$. Also, the mechanical impedance of the composites varies as a function of the external magnetic field resulting from the mechanical stress. However, this effect is not regarded as the dominant one above that of the magnetic-field-induced magnetoelectric impedance change. We notice that the linear transfer function for each modulation mode was measured at first since the parametric modulation is based on the detection of its change. The linear relation and the latter are required to evaluate the relative non-linearity factors.

For the **M/E** modulation, the magnetic excitation was achieved via the same custom-built modulation coil that was used above for the **M/M** mode. In this case, the coil was used to apply a relatively high frequency excitation magnetic field along the sensor length. Thus, the magnetic domains rotate and line-up with the external magnetic excitation. In particular, the magnetoelastic domain wall motion changes the deformation of the sensor via Joule and inverse piezomagnetic effects. For sub-resonant excitation frequencies, the Joule effect was dominant with regards to the magnetic induced deformations. This can then be used for the passive detection mode of the ME laminate under a bias magnetic field. This field can shift the working point into a dynamical linear regime. However, at the resonant excitation frequency of the ME composite, the magnetoelastic domains are forced to move synchronously with the external applied magnetic field. Thus, the inverse piezomagnetic effect becomes the dominant effect. Therefore,

TABLE IV
 MODULATION TRANSFER FUNCTION AND EQUIVALENT MAGNETIC NOISE SPECTRAL DENSITY FOR FOUR MODULATIONS

Modulation Mode	Sensitivity	Equivalent magnetic noise
M/M		
M/E		
E/M		
E/E		

Red circles, black points, triangles are the near carrier resonance measurement values, the predicted values (*cf.* theoretical equations) and the demodulated values, respectively.

a direct ME modulation can then be achieved at its first harmonic frequency without any magnetic bias. In the piezoelectric layer, the induced electric charges are collected

across a pair of interdigital electrodes. Kapton films with high resistivity, low electric dissipation loss factor and good thermo/hydro-stability were bonded to the piezoelectric layers

TABLE V
DEMODULATION TRANSFER FUNCTION AND EQUIVALENT MAGNETIC NOISE

Modulation Mode	Sensitivity	Equivalent magnetic noise
M/M		
M/E		
E/M		
E/E		

The black solid and dashed lines are the measurement and predicted responses (based on the model and results given in Table IV), respectively.

to protect these fragile layers from mechanical cracks as well as to incorporate the interdigital electrodes. These electrodes were connected to a classical charge amplifier [27], [28] with a resistance of $R_I (= 10 \text{ G}\Omega)$ and a capacitance of

$C_I (= 100 \text{ pF})$. The basic relation between the input charge Q_{ex} and output voltage U_{ex} is given by $U_{ex} = Q_{ex} / C_I$. With the objective of developing a technique for quantitative measurements of the attenuation, an attenuation factor Att_{ME}

was defined. This factor can be experimentally confirmed by the calculated and measured carrier output amplitudes for the **M/E** modulation. Moreover, the number of inter-digital electrodes, N_p , should also be considered for calculations. This number determines the efficiency of the charge detection by the piezoelectric layer. The nonlinear factor for the magnetic field can be defined by the ratio of equivalent side-band input magnetic field to the low frequency magnetic field. This can be further deduced as a formula of the sideband output signal amplitude U_2 , the output carrier amplitude U_{ex} and the reference magnetic field. Thus, the magnetic nonlinearity factor was defined as $\eta_1 = \frac{H_2}{H} / H_{ex} = \frac{2U_2}{U_{ex}H}$, as summarized in

Table III. Considering the number of inter-digital fingers N_p of the electrodes, the attenuation and nonlinear factors, the transfer function for the low frequency magnetic field and the output voltage noise density can be given as

$$Tr_{M/E} = \frac{N_p}{\mu_0 l_p C_1} \eta_1 \varphi_m \varphi_p C_{mech}^{EH} H_{ex} Att_{ME} \quad (12)$$

and

$$u_{n_f_M/E} = \frac{N_p}{l_p C_1} (\kappa_1 + \psi_1) \varphi_m \varphi_p C_{mech}^{EH} H_{ex} f_{n_C_{mech}} Att_{MFE}, \quad (13)$$

which induces an attenuation factor Att_{ME} for the magnetic field transfer function and an attenuation factor Att_{MFE} for the mechanical force.

These attenuation factors define the uncertainty for the transmission of a low frequency force. The equivalent magnetic noise spectral density can then similarly be expressed by the ratio between the output voltage noise and the transfer function as $b_{n_M/E} = \frac{u_{n_f_M/E}}{Tr_{M/E}}$. By applying a low reference

field, the sensitivity and noise was investigated as a function of the amplitude of the excitation field. Table IV shows the transfer functions, the output voltage noise spectral densities and the equivalent magnetic noise densities for this low frequency reference. However, a noise increase can be noticed in Table IV for higher excitation field. The ratio of the ME hysteresis loss energy to the total energy determines the noise level at a given excitation frequency. We believe that the increase of this ratio results from an excess noise increase. Table V shows the transfer functions, the output voltage noise spectral densities and the equivalent magnetic noise densities as a function of frequency for the low frequency magnetic reference, after the demodulation process. The transfer function is nearly constant over the measurement bandwidth from 0.1 Hz to 100 Hz. We notice that the predicted mechanical limit is a constant from the dashed lines in Table V. However, for stronger excitation amplitudes, the measured noise curves are higher than the predicted ones. This is due to the growth of the mechanical hysteresis loss. Thus, it is necessary to choose the optimal excitation amplitude so that the intrinsic noise of the composite can be discerned from the noise contribution of the detection electronics.

Presented in Table II is the experimental configuration for the converse ME modulation or so-called **E/M** modulation. A pair of Helmholtz coils generates a reference low frequency magnetic field along the longitudinal sensing direction of the ME composite. A voltage generator was then used to produce an excitation field across the interdigital electrodes in the in-plane, longitudinal direction. A voltage amplifier with a gain of $G_V (= 35)$ was used to amplify the low frequency field from an N_m turns home-made coil. The output voltage corresponding to the low frequency field, the excitation carrier and the modulation signal are defined respectively as U_1 , U_{ex} and U_2 . The transfer function and the output voltage noise spectral density can be calculated by

$$Tr_{E/M} = G_V \times N_m \frac{2\pi f_{ex}}{\mu_0 l_m} (2\varphi_m \tau_1) \varphi_m \varphi_p C_{mech}^{EH} E_{ex} Att_{EM} \quad (14)$$

and

$$u_{n_f_E/M}(f) = G_V \times N_m \frac{2\pi f_{ex}}{l_m} (\kappa_1 + \tau_1) \varphi_m \varphi_p C_{mech}^{EH} E_{ex} f_{n_C_{mech}} Att_{EFM} \quad (15)$$

where an attenuation factor Att_{EM} for the magnetic field transfer function and an attenuation factor Att_{EFM} for the mechanical force are both induced.

The equivalent magnetic noise spectral density can be expressed by the ratio between the output voltage noise and the transfer function as $b_{n_E/M} = \frac{u_{n_f_E/M}}{Tr_{E/M}}$. The nonlinear

term $2\varphi_m \tau_1$ for the **E/M** modulation can be calculated by

$$2\varphi_m \tau_1 = \frac{H_2}{E_{ex}} / H = \frac{2U_2}{U_{ex}H}$$

with measured parameters. By using a 2 Hz reference field, the sensitivity and noise were investigated as a function of the excitation amplitude of the carrier. Shown in Table IV are the transfer functions, the output voltage noise spectral densities and the equivalent magnetic noise spectral densities as a function of amplitude for a low frequency reference. The values of the transfer functions are linearly proportional to the amplitude of the excitation fields. Clearly, the noise contribution from the detection electronics dominates the total output noise level for low amplitude excitation signals. However, the loss energy increased faster than the stored one. This results an increase of the loss factor for stronger excitations. Table V shows the transfer functions, the output voltage noise spectral densities and the equivalent magnetic noise densities as a function of frequency of the reference field for the **E/M** modulation. Similarly to the direct ME modulation, a low-pass filter of 781 Hz serves in the demodulation process for the synchronism detection.

Table II also illustrates the setup configuration of the magneto-capacitance modulation for sensing low frequency magnetic fields. Unlike the direct and converse ME modulations, the frequency of the magnetostriction was readily doubled in the ME composite. This is because of the reversibility of the magnetic domain wall motion for zero biased magnetic oscillations at low frequencies. The

modulation process occurs in the piezoelectric layers. As known, there exists a part of the electric domain that can be changed by the mechanical strain or stress, which can be regarded as the origin of the stress-dielectric effect. The magnetic field induced electric capacity change, for the case of a magnetoelectric thin film composite, should be thoroughly treated as a strain (stress) induced dielectric effect, as there is no direct response of the electrical capacitance to the external magnetic fields in the ME composite. Thus, the magneto-elastic coupling is important for this detection mode since the variance of the dielectric coefficient is principally influenced by the state of stress resulting in the ferromagnetic phase. A magnetic bias can be applied to the ferromagnetic layer by shifting the working point, so that the magnetic induced strain can be maximized. In our experiments, a magnetic bias was chosen for investigating the sensitivity and noise behavior for magneto-capacitance modulation [29], [30]. This magnetic bias was applied to eliminate the frequency doubling of the reference signal and to enhance the sensitivity. The same charge amplifier as in the M/E modulation was used to amplify the low frequency signal from the generated charges with a resistance and a capacity in parallel. A voltage generator was connected onto the positive input for generating the excitation electric field E_{ex} across the attached inter-digital electrodes by applying an oscillation voltage $U(E_{ex})$. The amplitudes of the output signals were U_{ex} , U_2 and U_1 corresponding to the excitation, modulation and reference signals, respectively. The transfer function and the output voltage noise spectral density can then be given by

$$Tr_{E/E} = \frac{N_p}{\mu_0 C_1} \gamma_1 A_p \varepsilon^S E_{ex} Att_{EE} = \gamma_1 \frac{CU_{ex}}{\mu_0 C_1} Att_{EE} \quad (16)$$

and

$$u_{n-f-E/E}(f) = N_p \frac{1}{I_p C_1} (\kappa_1 \varphi_p + \gamma_1) \varphi_p C_{mech}^{EH} E_{ex} f_{n-C_{mech}} Att_{EFE}, \quad (17)$$

where an attenuation factor Att_{EE} for the magnetic field transfer function and an attenuation factor Att_{EFE} for the mechanical force are both induced.

The equivalent magnetic noise spectral density can be expressed by the ratio between the output voltage noise and the transfer function $b_{n-E/E} = \frac{u_{n-f-E/E}}{Tr_{E/E}}$. The nonlinear term γ_1

for the magneto-capacitance modulation was calculated by $\gamma_1 = \frac{E_2}{E_{ex}} / H = \frac{2U_2}{U_{ex}H}$ using measured parameters, where E_2 is

the equivalent electric field for the modulation signal. A low frequency magnetic field was applied on the ME composite to investigate the transfer functions and noise behavior by varying the amplitude of the excitation as shown in Table IV. A gap of several orders of magnitude can be seen in the equivalent magnetic noise spectral density of the corresponding figure in Table V. Therefore, we can conclude that thermal-mechanical fluctuations are not the dominant noise source for the magneto-capacitance modulation, presently. Table V again shows the transfer function, the output voltage noise spectral density and the equivalent magnetic noise spectral density as a function of frequency for the low frequency signals. In general, the sensitivity was dominated by the magneto-elastic coupling and the stress induced piezoelectric coefficient. The investigations of the sensitivity, output voltage noise and the equivalent magnetic noise spectral densities as a function of frequency are given in Table V. A gap between the measured and theoretical curves was also observed as a function of frequency.

TABLE VI
TRANSFER FUNCTION, OUTPUT VOLTAGE NOISE AND EQUIVALENT MAGNETIC NOISE SYNTHESIS

		M/M	M/E	E/M	E/E
Magnetic transfer function (V/T)	Predicted*	365	66.700	1.1 10 ⁶	288
	Measured	267	75.000	0.66 10 ⁶	319
Output voltage noise spectral density ($\mu\text{V}/\sqrt{\text{Hz}}$)	Predicted*	0.08	7.8	11.3	8.97 10 ⁻³
	Measured	6.5	7	42.2	1.64
Equivalent magnetic noise spectral density (pT/ $\sqrt{\text{Hz}}$)	Predicted*	220	114	10	3.3
	Measured	22.600	89	68.2	5.290
Power consumption (mW)		High (~100)	High (~100)	Low (~10)	Low (~10)
Magnetic bias for best sensitivity		Unclear	≈ 0	≈ 0	H_{dc}
Vibration sensitivity		Medium	Weak	Weak	Strong
Stability in time		Weak	Strong	Strong	Weak

TABLE VII
SYMBOL AND DEFINITION

Parameter	Symbol	Definition	Parameter	Symbol	Definition
Magnetic	B	Magnetic induction	Piezomagnetic	$d_{33,m}$	Piezomagnetic coefficient
	H	Magnetic field		$k_{33,m}$	Piezomagnetic coupling coefficient
	ν_1	Magnetic nonlinear factor		η_1	Magnetostrictive nonlinear factor
	μ	Magnetic permeability		η_1^*	Piezomagnetic nonlinear factor for a magnetic field
	Ψ	Magnetic flux		τ_1	Piezomagnetic nonlinear factor for a stress
Electric	D	Electric induction	Piezoelectric	$d_{33,p}$	Piezoelectric coefficient
	E	Electric field		$k_{33,p}$	Piezoelectric coupling coefficient
	U	Voltage		γ_1	Piezoelectric nonlinear factor to stress
	I	Current		φ_p	Electroelastic coupling factor
	Q	Charge			
	ε	Permittivity			
Elastic	C_{mech}^{EH}	Mechanical capacity	Geometric	A	Cross section area
	F	Force		l	Length
	f_n	Force noise SD		n	Thickness ratio
	S	Strain		t	Thickness
	s_{33}	Flexibility coefficient		V	Volume
	T_m, T_p	Stress in ferromagnetic and piezoelectric layers		w	Width
	ν_1, ν_2	Vibration speed			
	κ_1	Mechanical nonlinear factor			
Charge amplifier	C_1	Feedback capacity	Performance	b_n	Equivalent magnetic noise SD
	R_1	Feedback resistance		$e_{n,f}, i_{n,f}$	Output electric noise SD
				T_r	Transfer function
			$u_{n,f}$	Amplifier output voltage noise SD	
			α_{ME}^{NL}	Nonlinear magnetoelectric coefficient	
Other Parameters	Att	Attenuation factor	Acronym	MM	Magnetic excitation magnetic detection
	f	Ordinary frequency		ME	Magnetic excitation electric detection
	Gv	Voltage amplifier gain		EM	Electric excitation magnetic detection
	j	Imaginary unit		EE	Electric excitation electric detection
	k_B	Boltzmann constant		M/M	Magnetization modulation
	N_m	Coil turn number		M/E	Magnetoelectric modulation
	N_p	Piezoelectric segment number		E/M	Converse Magnetoelectric modulation
	ω	Angular frequency		E/E	Magneto-capacitance modulation
	T	Temperature		M/F/M	Magnetization modulation for a force
	$\tan\delta$	Loss factor		M/F/E	Magnetoelectric modulation for a force
				E/F/M	Converse magnetoelectric modulation for a force
				EFE	Magneto-capacitance modulation for a force
		SD	Spectral density		

The origin of this excess noise is from the detection system. This is experimentally and theoretically confirmed in [31]. The transfer capacity, output voltage noise and equivalent magnetic noise levels are presented in Table VI. Here, the noise sources and noise amplification from the detection electronics were considered as the dominant contributions to the equivalent magnetic noise. To summarize, the used parameters and their definitions are given in the Table VII.

IV. CONCLUSION

In summary, the dynamic sensitivity and noise floor of a long type, sandwich-like, push-pull-structured magnetostrictive-piezoelectric composite has been theoretical evaluated and measured. The theoretical model was based on an equivalent circuit model, which was extended to nonlinear modulation techniques. In addition, thermally induced mechanical fluctuations and their contribution to the total

performance of magnetic field sensing has been investigated. The modeling results were adapted to the measured ones. Equivalent magnetic noise levels were measured using either magnetic or electric field excitations with a charge amplifier or a pick-up coil detection system as required by the corresponding modulation methods. Presently, the direct (M/E) and converse magnetoelectric (E/M) modulations are expected to be the intrinsic mechanical loss under a frequency excitation field. Further research will focus on the mechanical uncertainties. To date, the noise contribution of the detection process and instrumentation electronics was the predominant noise source for the magnetization modulation (M/M) and the magneto-capacitance (E/E) modulation. For the other two methods, the sensor sensitivities should be enhanced in order to attain the intrinsic sensor noise. To this end, the noise from the detection process should be further reduced in the future research.

ACKNOWLEDGMENT

The authors would like to thank ONR global for support of this work.

REFERENCES

- [1] J. Ryu, S. Priya, K. Uchino, and H. Kim, "Magnetolectric Effect in Composites of Magnetostrictive and piezoelectric Materials," *Journal of Electroceramics*, vol. 8, pp. 107-119, 2002
- [2] C. Nan, M. I. Bichurin, S. Dong, D. Viehland, and G. Srinivasan, "Multiferroic magnetolectric composites: Historical perspective, status, and future directions," *Journal of Applied Physics*, vol. 103, p. 031101, 2008
- [3] J. L. Prieto, C. Aroca, P. Sanchez, E. Lopez, and M. C. Sanchez, "Current effects in magnetostrictive piezoelectric sensor," *Journal of Magnetism and Magnetic Materials*, vol. 174, pp. 289-294, 1997
- [4] S. Dong, J. Zhai, J. Li, and D. Viehland, "Near-ideal magnetolectricity in high-permeability magnetostrictive/piezofiber laminates with a (2-1) connectivity," *Applied Physics Letters*, vol. 89, p. 252904, 2006
- [5] J. Zhai, S. Dong, Z. Xing, J. Gao, J. Li, and D. Viehland, "Tunable magnetolectric resonance devices," *Journal of Physics D: Applied Physics*, vol. 42, p. 122001, 2009
- [6] X. Zhuang, M. Lam Chok Sing, C. Cordier, S. Saez, C. Dolabdjian, L. Shen, J. Li, M. Li, and D. Viehland, "Evaluation of applied axial field modulation technique on ME sensor input equivalent magnetic noise rejection," *IEEE Sensors Journal*, vol. 11, pp. 2266-2272, 2011
- [7] S. M. Gillette, A. L. Geiler, D. Gray, D. Viehland, C. Vitteria, and V. G. Harris, "Improved sensitivity and noise magneto-electric magnetic field sensor by use of modulation AC magnetostriction," *IEEE Magnetic Letters*, vol. 2, p. 2500104, 2011
- [8] H. B. Wang, and Z. H. Feng, "A highly sensitive magnetometer based on the Villari effect," *IEEE Transactions on Magnetics*, vol. 49, p. 1327, 2013
- [9] M. D. Mermelstein, and A. Dandridge, "Low frequency magnetic field detection with a magnetostrictive amorphous metal ribbon," *Applied Physics Letters*, vol. 51, p. 545, 1987
- [10] Q. Liu, X. Bian, J. Zhou, and P. Liu, "Colossal magnetodielectric effect caused by magnetolectric effect under low magnetic field," *Bulletin of Materials Science*, vol. 34, pp. 283-286, 2011
- [11] M. Maglione, W. Zhu, and Z. H. Wang, "Evidence of a strong magnetic effect on the impedance of integrated piezoelectric resonators," *Applied Physics Letters*, vol. 87, p. 092904, 2005
- [12] N. A. Pertsev, S. Prokhorenko, and B. Dkhil, "Giant magnetocapacitance of strained ferroelectric-ferromagnetic hybrids," *Physical Review B*, vol. 85, p. 134111, 2012
- [13] Y. Wang, D. Gray, D. Berry, J. Gao, M. Li, J. Li, and D. Viehland, "An extremely low equivalent magnetic noise magnetolectric sensor," *Advanced Materials*, vol. 23, pp. 4111-4114, 2011
- [14] J. Gao, Y. Shen, Y. Wang, P. Finkel, J. Li, and D. Viehland, "Magnetolectric bending-mode structure based on Metglas/Pb(Zr, Ti)O₃ fiber laminates," *IEEE Transactions on ultrasonics, ferroelectrics, and frequency control*, vol. 58, p. 1545, 2011
- [15] S. Dong, J. Zhai, J. F. Li, and D. Viehland, "Magnetolectric gyration effect in Tb_{1-x}Dy_xFe_{2-y}/Pb(Zr, Ti)O₃ laminated composites at the electromechanical resonance," *Applied Physics Letters*, vol. 89, p. 243512, 2006
- [16] H. Zhou, C. Li, L. Xuan, J. Wei, and J. Zhao, "Equivalent circuit method research of resonant magnetolectric characteristic in magnetolectric laminate composites using nonlinear magnetostrictive constitutive model," *Smart Materials and Structures*, vol. 20, p. 035001, 2011
- [17] M. I. Bichurin, V. M. Petrov, and G. Srinivasan, "Theory of low-frequency magnetolectric effects in ferromagnetic-ferroelectric layered composites," *Journal of Applied Physics*, vol. 92, p. 9681, 2002
- [18] S. Dong, J. Li, and D. Viehland, "Magnetolectric couplings, efficient, and voltage gain effect in piezoelectric-piezomagnetic laminate composites," *Journal of Materials Science*, vol. 41, pp. 97-106, 2006
- [19] F. Yang, Y. M. Wen, P. Li, M. Zheng, and L. X. Bian, "Resonant magnetolectric response of magnetostrictive/piezoelectric laminate composite in consideration of losses," *Science and Actuators A*, vol. 141, pp. 129-135, 2008
- [20] A. Mougin, M. Cormier, J. P. Adam, P. J. Metaxas, and J. Ferre, "Domain wall mobility, stability and walker breakdown in magnetic nanowires," *Europhysics Letters*, vol. 78, p. 57007, 2007
- [21] N. L. Schryer, and L. R. Walker, "The motion of 180° domain walls in uniform dc magnetic fields," *Journal of Applied Physics*, vol. 45, p. 5406, 1974
- [22] X. Cui, and S. Dong, "Theoretical analyses on effective magnetolectric couplings coefficients in piezoelectric/piezomagnetic laminates," *Journal of Applied Physics*, vol. 109, p. 083903, 2011
- [23] X. Zhuang, C. Cordier, S. Saez, M. Lam Chok Sing, C. Dolabdjian, J. Gao, J. F. Li, and D. Viehland, "Theoretical analysis of the intrinsic magnetic noise spectral density of magnetostrictive-piezoelectric laminated composites," *Journal of Applied Physics*, vol. 109, p. 124512, 2011
- [24] X. Zhuang, M. Lam Chok Sing, C. Cordier, S. Saez, C. Dolabdjian, J. Das, J. Gao, J. Li, and D. Viehland, "Analysis of noise in magnetolectric thin-layer composites used as magnetic sensor," *IEEE Sensors Journal*, vol. 11, p. 2183, 2011
- [25] X. Zhuang, M. Lam Chok Sing, C. Dolabdjian, "Investigation of the near-carrier noise for strain-driven ME laminates by using cross-correlation techniques," *IEEE Transactions on Magnetics*, vol. 49, pp. 120-123, 2012
- [26] D. C. Jiles, "Theory of the magnetomechanical effect," *Journal of Physics D: Applied Physics*, vol. 28, pp. 1537-1545, 1995
- [27] Z. P. Xing, J. Y. Zhai, S. X. Dong, J. F. Li, D. Viehland, and W. G. Odendaal, "Modeling and detection of quasi-static nanotesla magnetic field variations using magnetolectric laminate sensor," *Measurement Science and Technology*, vol. 19, p. 015206, 2008
- [28] J. Jiao, L. Li, B. Ren, H. Guo, H. Deng, W. Di, X. Zhao, W. Jing, and H. Luo, "Parallel multilayer magnetolectric composite based on (1-x)Pb(Mg_{1/3}Nb_{2/3})-xPbTiO₃ and Terfenol-D coupled with charge mode amplifier," *Journal of Applied Physics*, vol. 111, p. 043909, 2012
- [29] C. Israel, V. M. Petrov, G. Srinivasan, and N. D. Mathur, "Magnetically tuned mechanical resonances in magnetolectric multilayer capacitors," *Applied Physics Letters*, vol. 95, p. 072505, 2009
- [30] L. Yang, J. Tang, W. Wang, X. Luo, N. Zhang, "The effect of magnetic field-tuned resonance on the capacitance of laminate composite," *Journal of Sensor Technology*, vol. 1, pp. 81-85, 2011
- [31] X. Zhuang, M. Lam Chok Sing, C. Dolabdjian, Y. Wang, P. Finkel, J. Li, and D. Viehland, "Sensitivity and noise evaluation of a bonded magneto(elasto)electric laminated sensor based on in-plane magneto-capacitance effect for quasi-static magnetic field sensing," to be published in *IEEE Transactions on magnetics*, 2014.